

A multiband patch antenna with embedded square split ring resonators in non-Homogeneous substrate

Shailesh M. Rao, Prabhugoud I. Basarkod

School of Electronics and Communication Engineering, REVA University, Bengaluru, India

Article Info

Article history:

Received Apr 20, 2020
Revised Dec 5, 2020
Accepted Mar 16, 2021

Keywords:

Dual substrate
Multiband
Permittivity
Square split ring resonator

ABSTRACT

The authors have attempted to influence an embedded square split ring resonator (SSRR) response in a stacked non-homogeneous substrate to demonstrate a quad-band antenna. The purpose is to produce multiband operations of a microstrip patch antenna. The highlighted factor is the effect of embedding an SSRR and the differing relative permittivity of the substrate on the side length of the SSRR. The analysis shows that a non-homogeneous dual substrate patch produces multiple bands compared to a single substrate patch antenna without any parameter change. A dual substrate antenna fabricated using FR4 and Rogers RT/Duroid 5880 copper clad sheets with a dimension of $85.6 \times 54 \times 0.908 \text{ mm}^3$ ($0.314\lambda_0 \times 0.198\lambda_0 \times 0.003\lambda_0$). The antenna resonates at 1.1, 2.45, 3.65 and 5.25 GHz in the L-, S- and C-bands. It is possible to employ the patch antenna in WLAN (dual-band) and WiMAX applications and suitable for mobile broadcast service at 1.1 GHz. The authors compare the simulated and measured results of a prototype in the article. The maximum measured gain is 5.48 dBi at 1.1 GHz and 4.025 dBi at 3.65 GHz. The measured bandwidth is 60 MHz (1.2%) at 5.25 GHz.

This is an open access article under the [CC BY-SA](#) license.



Corresponding Author:

Shailesh M. Rao
School of Electronics and Communication Engineering
REVA University
Rukmini Knowledge Park, Kattigenahalli, PO Yelahanka, Bengaluru, India
Email: marolishaileshrao@hotmail.com

1. INTRODUCTION

The need to develop novel antennas for modern generation electronic devices poses a challenge to antenna engineers. Creating new and innovative designs to support wideband/multiband operations is essential. Performance in a compact size is a crucial factor in making an antenna appealing. The various WLAN bands, WiMAX and RFID, are of interest for many applications concerning mobile electronic devices, item identification, tracking, access control and other such applications.

A report is available on a microstrip antenna on an FR4 substrate of 0.8 mm thick with wideband characteristics and decent gain values. The antenna operates from 0.8 to 6.05 GHz and has a bandwidth of 5.25 GHz bandwidth [1]. A meandered stripline feed and H/U-type slits on the radiating plane are used in this design along with defected ground to obtain broadband characteristics. In literature, we see a great deal of effort in studying the various approaches to improve bandwidth in a compact form factor and facilitate a patch antenna's operation in multiple bands. The metallic conductors' magnetic behaviour report revolutionised devices' design in radio frequency and optical applications [2]. The authors discuss an antenna using a triangular split ring resonator [3] with a low measured gain. A triple-band antenna is reported with a reconfigurability feature and split ring resonator in [4] with a gain of 3 dBi. A T-shaped structure loaded with meander line stubs on a small area operates in multiple bands (L/S/C bands) and has decent bandwidths and a

maximum gain of 3.4 dBi [5]. H. Xiong *et al.* [6] discusses a UWB antenna using metamaterials with 267% impedance bandwidth and excellent gain. However, the antenna radiation performance is affected in some frequencies due to high levels of cross-polarisation. Many instances of the use of complementary split ring resonators in several investigations are available.

Research highlights their efficacy in improving microstrip patch antennas' performance [7], [8]. A circular patch antenna loaded with CSRR operates in two frequency bands producing circular polarisation is presented in [9]. R. O. Ouedraogo *et al.* [10] and R. O. Ouedraogo and E. J. Rothwell [11] discuss an SRR metallic ring embedded between substrate material of the same type (Rogers RT/Duroid 5870 and Rogers RT/Duroid 5880, respectively). The article discusses the advantage of using an SRR to reduce the size of the circular path without compromising on the overall radiation performance [10]. However, the reported gain is small due to miniaturisation.

J. C. Xing Zhao and Youngki Lee [12] employs an SRR array embedded between two FR4 substrates to reduce the antenna's size while retaining the fractional bandwidths. M. Shailesh Kumar and Prabhugoud I. Basarkod [13] discusses a stacked multiple substrate antenna working in the UHF band producing decent radiation characteristics. A couple of articles discuss antennas using stacked and bonded homogeneous substrates. The article does a comprehensive analysis of a CPW-fed antenna with resonators on different substrate materials leading to miniaturisation [14]. Though the radiation characteristics have improved, this antenna's peak gain even after employing the enhancement technique is -1.22 dBi. A stacked multi-structure circular patch with air dielectric operating in the UWB frequency is presented in [15] with a measured bandwidth of 3.68 to 13.8 GHz (115.8%). C. D. R. R. Prasad Rao and Budumuru Srin [16] provides proof for improving a microstrip antenna's bandwidth with a multilayer substrate. An article presents AMC's use at 5.8 GHz for WBAN application to reduce the back lobe [17]. Effective use MTM with photonic bandgap structures to improve isolation between the transmit and receive section demonstrated by the authors [18]. Using slots and defective ground structure to suppress harmonics is verified using a prototype based on numerical analysis to achieve the desired result [19]. A THz regime novel high-gain metasurface (acting as an AMC) polyimide on-chip antenna with a microstrip feed line in the bottom substrate with a gain of 8.15 dBi is presented by M. Alibakhshikenari [20].

M. Alibakhshikenari *et al.* [21] discusses a 2x2 microstrip patch antenna with super-wide frequency bandwidth. The inclusion of slot combined with metamaterial loading provides a fractional bandwidth of 142.85%, improved gain and enhanced radiation efficiency. The authors present a novel slot antenna with two excitation ports for an extended bandwidth in [22]. An H-shaped slit provides isolation between the radiators as per design. Metasurfaces intelligently used to suppress mutual coupling between adjacent radiating elements in MIMO antennas [23]. The reduction of surface wave aids in improving the bandwidth and reduces the cross-coupling factors in the radiated beam. Substrate integrated waveguide and metasurface feature to reduce the unwanted mutual coupling in a 34x34 array antenna operating in the Terahertz band [24]. A decoupling slab with an embedded MTM electromagnetic bandgap structure and a fractal isolator enhance isolation between the radiators discussed in [25] and [26].

In this proposed work, the focus is on a microstrip patch antenna working in L-, S- and C- bands of the frequency spectrum with an embedded square split ring resonator (SSRR) array. The SSRR array is between two substrates of different relative permittivity values. The article emphasises using embedded SSRR in a dual dielectric non-homogeneous substrate to operate in multiple bands. The main advantage of using non-homogeneous substrates is reducing the side lengths of the resonating metallic inclusions. The detailed discussions on the matter follow in the subsequent sections. The proposed design uses bonded substrates to enhance the radiation characteristics; hence, the practical volume is small compared to an antenna employing a superstrate. The designed antenna resonates at four different frequencies in L-, S- and C- bands. The gain, bandwidth, reflection coefficient, and radiation pattern of the fabricated antenna closely match the simulated values.

The designed antenna is suitable for use in WLAN (802.11a/b/g/n/j/ac/ax) and WiMAX (802.11y) applications. The 1.1 GHz frequency is also suitable for federal and non-federal aviation service and mobile broadcasting services. Ansys HFSS software, a full-wave EM solver, is used to carry out the design's numerical analysis with an extensive parametric study. Open source software Veusz used to prepare the graphical presentations in the paper.

2. DUAL SUBSTRATE ANTENNA WITH EMBEDDED SSRR ARRAY

2.1. Dual substrate patch antenna design

As a convention, most of the approaches to design and fabricate patch antennas have delved into single substrate antennas due to ease of fabrication and related economics. One of the popular substrates for development is Flame Retardant Epoxy Glass substrate FR4. Rogers Corporation manufactures substrates for antenna applications

with some superior performance characteristics under their RT/Duroid product line. Researchers have used these substrate materials to develop their designs extensively. The design of multi-substrate antennas can be with bonded structures [13], [14], and [16]. It could also be a superstrate [7], [27], [28].

In this paper, a dual substrate antenna designed with FR4 ($\epsilon_r=4.4$, $\tan \delta=0.02$) and Rogers RT/Duroid 5880 ($\epsilon_r=2.2$, $\tan \delta=0.00019$) as the substrate material is studied. The dimension of the antenna is $85.6 \times 54 \times 0.908 \text{ mm}^3$ ($0.314\lambda_0 \times 0.198\lambda_0 \times 0.003\lambda_0$). The top layer is of FR4, which is 0.4 mm thick (Layer 1), and the bottom layer is RT/Duroid 5880, which is 0.508 mm thick (Layer 2). The first stage of development was designing the patch antenna on a single substrate FR4 material of thickness 0.8mm. Figure 1(a) shows the antenna schematic. This antenna resonated at only one frequency (3.9 GHz). In the next step, the addition of 0.508 mm thick layer of Rogers RT/Duroid 5880 done below the FR4 layer (0.4mm thick). This structure yielded resonance at 2.45/3.6/5.21/5.93/6.16 GHz. In the next step, an SSRR array incorporated between the substrate layers leading to a change of the resonant bands to four frequencies (1.1/2.45/3.65/5.25 GHz) and at the same time suppressing the undesired frequency bands. The later sections in the article have a detailed discussion on this aspect.

The patch dimensions are calculated based on formulas for deriving the same as described in [29]. The transmission line model adopted to calculate the dimensions of the patch antenna. The effective relative permittivity (ϵ_{ref}) of the antenna when the ratio $w/h>1$ is given in (1)

$$\epsilon_{ref} = \frac{\epsilon_r+1}{2} + \frac{\epsilon_r-1}{2} \left[1 + 12 \frac{h}{w} \right]^{-1/2} \quad (1)$$

The width of the patch (w_p) is related to the resonant frequency (f_r), the velocity of light in free space (v_0) and relativity permittivity (ϵ_r) by the relationship in (2),

$$w_p = \frac{v_0}{2f_r} \sqrt{\frac{2}{\epsilon_r+1}} \quad (2)$$

Consider the dominant mode of excitation (TM_{10}) of the patch antenna, and the patch length is given by (3) as,

$$l_p = \frac{c}{2f_r \sqrt{\epsilon_{ref}}} \quad (3)$$

The design utilises inset feed to obtain wideband impedance matching. The calculation of the inset length (y_0) into the patch utilising in (4),

$$R_{in(y=y_0)} = R_{in(y=0)} \cos^2 \left(\frac{\pi}{l_p} y_0 \right) \quad (4)$$

Where, $R_{in(y=y_0)}=50 \Omega$ and $R_{in(y=0)}$ is the impedance at the edge of the patch.

After obtaining the initial values, the dimensions iteratively modified to obtain the best possible EM solver results for the desired band of frequencies. The list of dimensions of the antenna and SSRR is in Table 1. Figure 2(a) depicts the top radiating patch of the antenna on FR4. Figure 2(b) shows the SSRR array's layout in the intermediate layer etched on the Rogers RT/Duroid 5880 substrate. Figure 2(c) shows the image of the antenna fabricated using the photolithographic process with the radiating patch and the SSRR array using the two-substrate materials. The two layers are stacked one over the other and bonded with glue to obtain a firm contact between the surfaces.

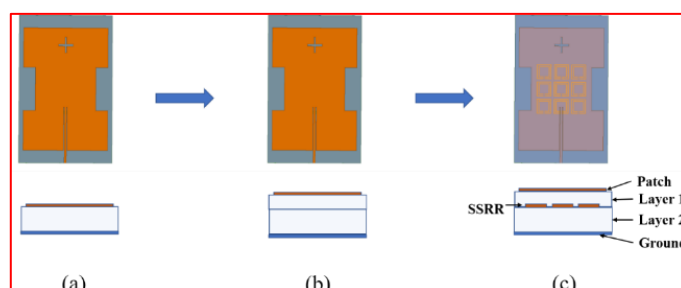


Figure 1. The evolution process of development of the embedded SSRR patch antenna (dimensions not to scale), (a) Patch antenna on a single substrate (FR4), (b) Patch antenna on dual substrate (FR4 and Rogers RT/Duroid 5880) (c) Patch antenna on a dual substrate with embedded SSRR

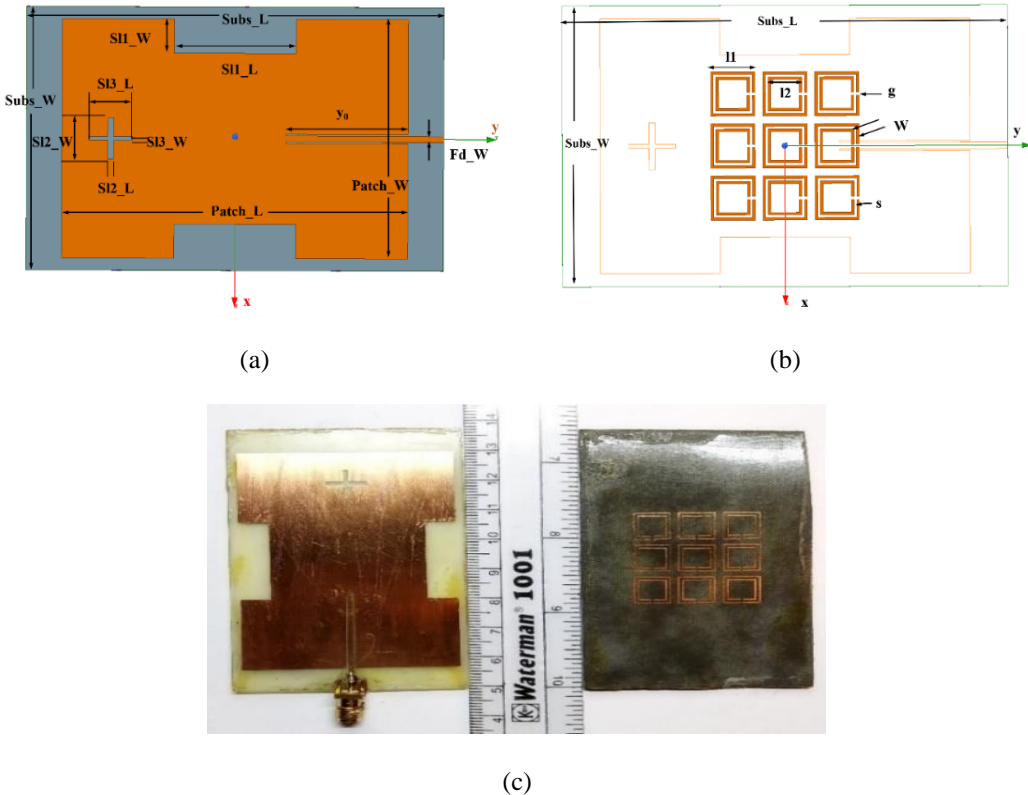


Figure 2. Embedded SSRR patch antenna, (a) The top layer with radiating patch and substrate dimensions, (b) The SSRR layer on Rogers RT/Duroid 5880, (c) Fabricated dual substrate microstrip patch antenna displaying the radiating patch and the intermediate SSRR array layer

Table 1. Dimensions of the antenna and SSRR

Parameter	Dimensions (mm)	Parameter	Dimensions (mm)
$Subs_L$	85.6	$SI2_W$	9
$Subs_W$	54	$SI3_L$	8.4
$Patch_L$	71	$SI3_W$	1.2
$Patch_W$	49	$y0$	25
$h1$	0.4	11	8.5
$h2$	0.508	12	6.9
$SI1_L$	25	W	0.5
$SI1_W$	7	s	0.3
$SI2_L$	0.8	g	0.6

2.2. Design of square split ring resonator

A metamaterial unit cell's performance and an array have been described based on the Kramers-Kronig relationship in [30]. Parameter retrieval based on the S-parameters of a unit cell metamaterial is discussed in detail [31], [32]. The above work explores structures exhibiting tuneable magnetic conductivity built from nonmagnetic conducting sheets. H. Chen *et al.* [33] refers to S-shaped resonators acting as left-handed materials without the aid of a wire to generate double negative values of EM parameters.

The etching of a 3x3 SSRR array on the Rogers RT/Duroid 5880 substrate's top surface is as per the design in the proposed work. Available literature talks about different types of resonant structures like circular, rectangular, triangular and other such shapes Shalini Sah and Malay R Tripath [34], Chaturvedi and Raghavan [35] to cite a couple of research articles. The reason for selecting a square resonator is that it requires a smaller dimension (side length) compared to a circular or any other such shape. Studies show that aligned split gaps of the rings in the same direction generates dual resonances in close range. Proximity double resonance is otherwise not possible in the complementary orientation of the split gaps. As shown in (5) gives the average length of the conductor l_{avg} [36],

$$l_{avg} = 4[l_1 - (N - 1)(s + W)] \quad (5)$$

$$\varepsilon_r^t = \frac{[\varepsilon_{r1} + \varepsilon_{r2} + 2]}{4} \quad (6)$$

where ε_r^t is the average relative permittivity of the dual substrate layer [37], N is the number of turns of the rings. The expression for effective relative permittivity (ε_{rsub}) of the substrates (7),

$$\varepsilon_{rsub} = 1 + \frac{2}{\pi} \arctan \left[\frac{h}{2\pi(w+s)} \right] (\varepsilon_r^t - 1) \quad (7)$$

With the help of the above equations, description of the capacitance and inductance of a metallic inclusion on a dielectric substrate is possible by the below-given as [36],

$$C_{SSRR} = \frac{N-1}{2} [2l_1 - (2N-1)(w+s)] C_0 \quad (8)$$

$$C_0 = \varepsilon_0 \varepsilon_{rsub} \frac{K(\sqrt{1-k^2})}{K(k)} \quad (9)$$

$$L_{SSRR} = \frac{\mu_0}{2} \frac{l_{avg}}{4} (4 \cdot 86) \left[\ln \left(\frac{0.98}{\rho} \right) + 1 \cdot 84\rho \right] \quad (10)$$

$$f_r = \frac{1}{2\pi\sqrt{L_{SSRR} \cdot C_{SSRR}}} \quad (11)$$

Where $h=h_1 + h_2$ is the total height of the substrate. ρ is the fill factor for the metallic inclusion on the dielectric substrate ($\rho=(N-1)(w+s)/[l_1-(N-1)(w+s)]$), K is the elliptic integral of the first kind. The variable k defines the lower integer number of the ratio $[s/(w+s)]$. L_{SSRR} is the inductance, and C_{SSRR} is the capacitance of the metallic inclusion, f_r is the resonant frequency of the SSRR structure based on the equivalent quasi-static model defined by the equations above. The calculated value of f_r as per (11) is 2.315 GHz. The average permittivity of the dual substrate stack calculated as per (6) is 2.15 (ε_r^t).

Figure 3 shows the unit cell in a waveguide medium set up to extract the S-parameters of the SSRR to evaluate the EM response, and the tutorial describes the method for extraction of S-parameters of a unit cell. The tutorial highlights the procedure for retrieval of permeability, permittivity and refractive index [38]. The extraction of the EM parameters is possible by the Nicholson-Ross-Weir (NRW) method or transmission-reflection (TR) method (two popular techniques of a couple of methods available). We make use of (12) and (13) to compute the refractive index (n) and impedance (z) of the metamaterial,

$$n = \frac{1}{kd} \cos^{-1} \left[\frac{1}{2S_{21}} (1 - S_{11}^2 + S_{21}^2) \right] \quad (12)$$

$$z = \sqrt{\frac{(1+S_{11})^2 - S_{21}^2}{(1-S_{11})^2 - S_{21}^2}} \quad (13)$$

Once the refractive index and impedance is known, the magnetic permeability (μ) of the SSRR is calculated by (14),

$$\mu = (n \times z) \quad (14)$$

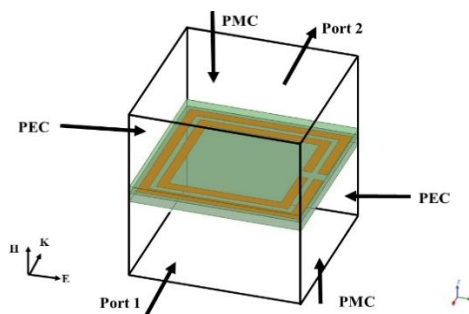


Figure 3. Design of unit cell of SSRR for extraction of S-parameters using waveguide setup

The plot of permeability response of the SSRR is in Figure 4. The real part of the structure's permeability is negative at 2.362 GHz and 3.628 GHz exhibiting the single negative material characteristic. The permeability response is nearly zero for a considerable range of frequencies in the 5-5.5 GHz band, as seen in Figure 4(a). Figure 4(b) describes the response of the SSRR in a configuration of a three-cell unit and 3x3 array. The mutual coupling factor between the rings contributes to the extended behaviour of the three-cell unit's permeability response and 3x3 array.

The use of two different substrates has resulted in smaller dimensions of the metallic inclusion's side length. A discussion on dielectric composition's effect on resonant frequencies of a metallic inclusion in the conference article [39] highlights the importance of dielectric composition. Embedding the SSRR structure between the two layers helps lower the resonance frequency than the same etched on a single substrate. The resonant frequency for a split ring resonator with a side length of the outer ring $l=8.5$ mm for a single cell is tabulated in Table 2 for different substrate material selections.

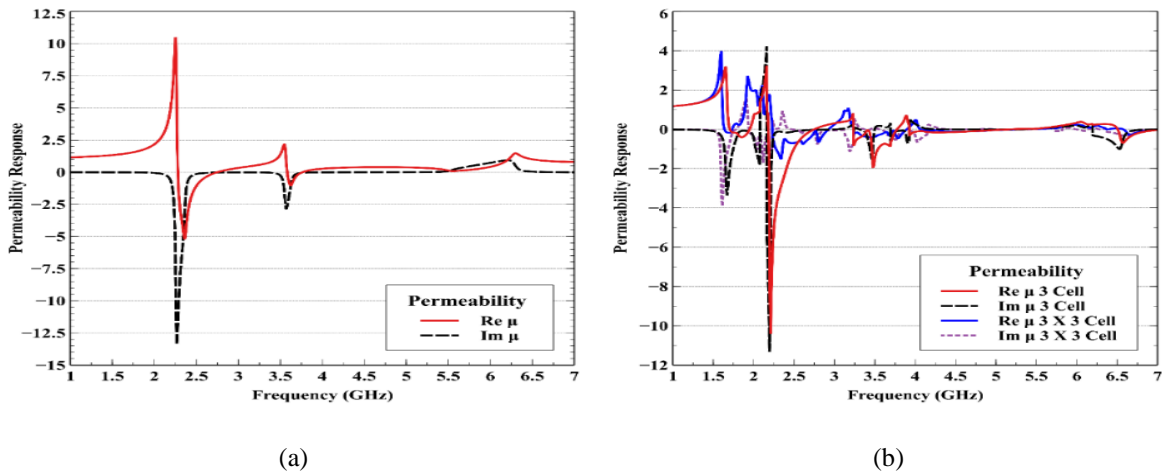


Figure 4. Permeability response of SSRR, (a) Response of single unit cell, (b) Response of 3-cell unit and 3x3 array

The resonant frequency values obtained indicate that the effect of non-homogeneous substrates on the resonant frequency is considerable. The result would be more profound at higher frequencies. Table 2 compares the proposed SSRR configuration and SRR response in terms of their resonance frequencies. As the reaction of metallic inclusions clearly illustrates that the SSRR produces dual resonance compared to SRR due to the combined effect of per unit capacitance and the gap capacitance. SRR produces a single lower resonant frequency for the given side length dimension. Hence, it is advantageous to incorporate in cases where a single resonance is required. Whereas the proposed SSRR produces dual resonance for the same structure due to the combined capacitive effect as stated above. Further size reduction is possible by selecting one material with higher relative permittivity (~ 10) and the other with a lower relative permittivity (~ 2). A 40% reduction in the resonance frequency in a few cases is achievable [39].

Table 2. The frequency response of proposed SSRR and SRR on different substrate materials

Substrate Type	Resonant frequency proposed SSRR (GHz)		Resonant Frequency SRR (GHz)
	f_{r1}	f_{r2}	
Rogers RT /Duroid 5880	3.22	5.188	2.854
FR4	2.578	4.3	2.284
FR4 + RT/Duroid 5880	2.362	3.628	2.034

3. RESULTS AND DISCUSSION

3.1. Reflection coefficient (S_{11})

A commercial solver based on the finite element method (FEM) (Ansys HFSS) assesses the antenna design numerically. Figure 5(a) depicts the antenna's numerical response under different material consideration for the design. The first case of design is when the antenna is on a single substrate (FR4)

material (0.8mm thick). The antenna produces resonance at 3.9 GHz only. The second case is the response depicted for a dual substrate antenna made up of FR4 and Rogers RT/Duroid 5880 without embedded SSRR.

The total thickness of the antenna substrate is 0.908 mm. We see in the second case that the antenna resonates at six frequencies (1.1/2.45/3.6/5.21/6.16 GHz) even though the radiating patch dimension is unaltered. It is due to the change in the effective relative permittivity of the substrate. The third case is that of a dual substrate antenna with embedded SSRR. The antenna resonates at four frequencies (1.1/2.45/3.65/5.25 GHz). In comparing the second and third case, the suppression of the frequency band's upper end (6.16 GHz) is due to the embedded SSRR. It is due to the attenuation induced by the real part of the embedded SSRR array's permeability (refer to Figure 4). Another factor is the improved reflection coefficient levels of the antenna with the SSRR compared to the one without SSRR due to metallic inclusion.

The reflection coefficient S_{11} of the fabricated dual substrate patch antenna with the embedded SSRR was measured using an Anritsu vector network analyser (VNA-S820E). Figure 5(b) shows the plot of the measurement. The measured reflection coefficient values closely match the numerical values at the various resonating frequencies. The magnitude of the measured reflection coefficient is slightly lower compared to the numerical results. Due to the inaccuracies of alignment and bonding of the two-substrate layers, cable/connector losses lead to the degradation in reflection coefficient values.

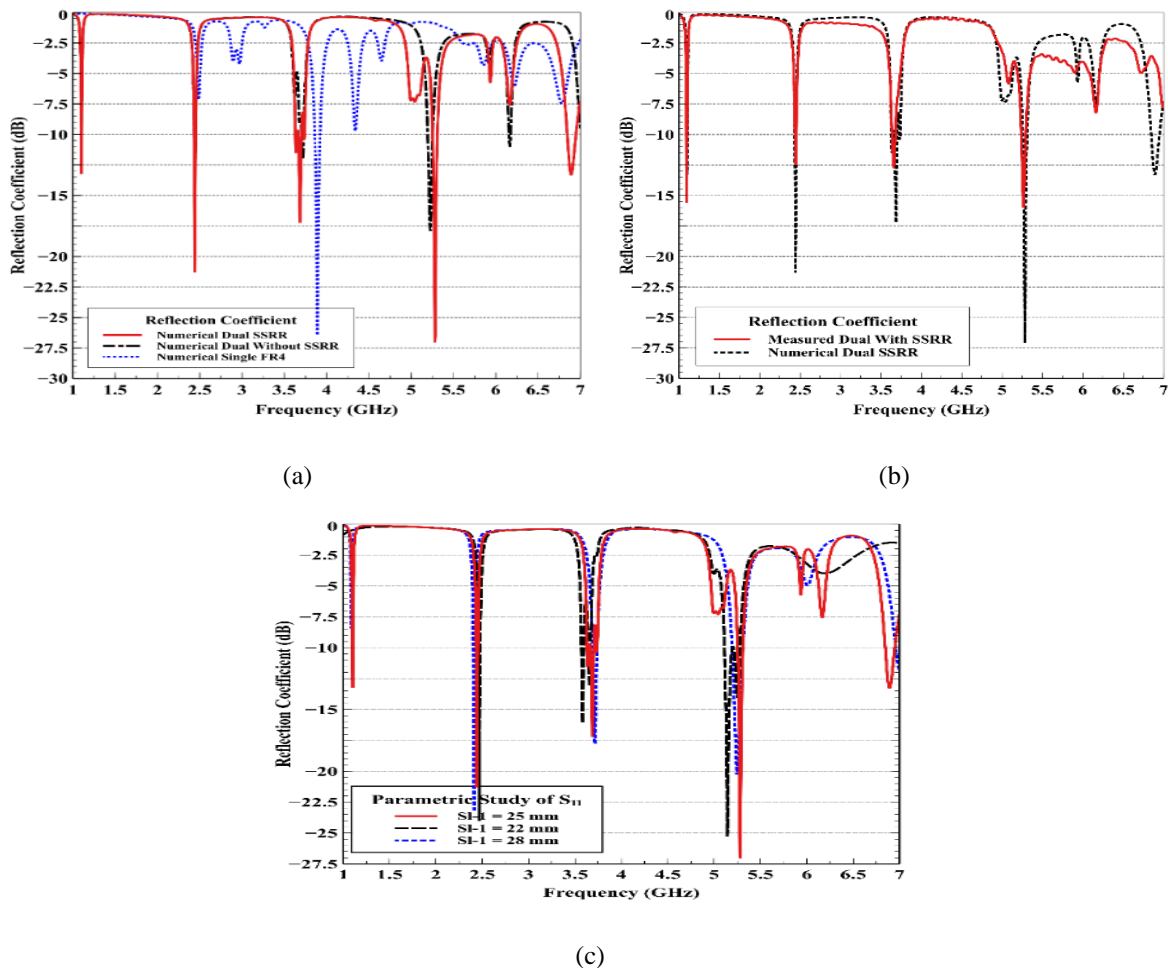


Figure 5. Reflection coefficient response (S11), (a) Results of the numerical analysis of the antenna structure with single substrate FR4, dual substrate without SSRR and dual substrate with embedded SSRR, (b) Comparison of the measured and simulated reflection coefficient of the dual substrate patch antenna with embedded SSRR, (c) Parametric analysis of slot length highlighting variations in S11

Table 3 tabulates the prototype antenna's measured bandwidth and the antenna's simulated bandwidth with and without an SSRR array. It is a proven fact that the bandwidth of a conventional microstrip patch antenna is directly proportional to the substrate's thickness. The antenna's impedance

bandwidth is lesser than other designs discussed in the literature, mainly due to two reasons. First, the antenna uses a relatively thin substrate (0.908 mm) compared to different models, which use 1.6 mm or higher thickness values. Second, the proposed design does not incorporate bandwidth enhancement techniques like meander lines or defective ground structure. We obtain better bandwidths for the non-homogenous structure compared to a single substrate antenna of comparable design parameters.

Parametric study of the antenna carried out by varying the slot length $SL1$ (varied between 22 mm to 28 mm). The results of the parametric analysis for the reflection coefficient is in Figure 5(b). The parametric study yielded the best results for a slot length of 25 mm for $SL1$.

Table 3. Tabulation of the measured and simulated bandwidth of the dual substrate patch antenna with embedded SSRR array

Frequency (GHz)	Measured Bandwidth (With SSRR) (MHz)	Simulated Bandwidth (With SSRR) (MHz)	Percentage Bandwidth (With SSRR) (Measured) (%)	Simulated Bandwidth (Without SSRR) (MHz)
1.1	9	8	0.82	6
2.45	18	22	0.74	21
3.65	45	42	1.23	20
5.25	60	55	1.2	60

3.2. Gain and efficiency of the antenna

The antenna response characterised in an anechoic chamber. The radiation measurement is done in a chamber of dimension $7 \times 4 \times 3 \text{ m}^3$. A distance of 5.5 m separates the AUT from the source that is a broadband horn antenna of linear polarisation. The antenna exhibits decent gain levels in the four frequency bands of interest. The plot of simulated and measured antenna gain is in Figure 6(a). Table 4 tabulates the gain values at the different resonant frequencies. The highlight of the design is decent gain values at different resonant frequencies by a thin substrate structure. It is due to the use of a dual substrate and the embedded SSRR. The use of low loss substrates like Rogers RT/Duroid 5880 and the SSRR enhances the patch antenna's gain.

The plot in Figure 6(b) depicts the microstrip patch antenna's radiation efficiency with embedded SSRR, and the efficiency of the antenna is 47% at 3.65 and 5.25 GHz. The efficiency at 1.1 and 2.45 GHz is 42.5 and 41%, respectively. The dual substrate antennas (with and without SSRR) shows a marked improvement in efficiency compared to the single substrate antenna printed on FR4 substrate (9% at 3.9 GHz). The use of second substrates aids in improving the overall radiation efficiency across the various resonance frequencies.

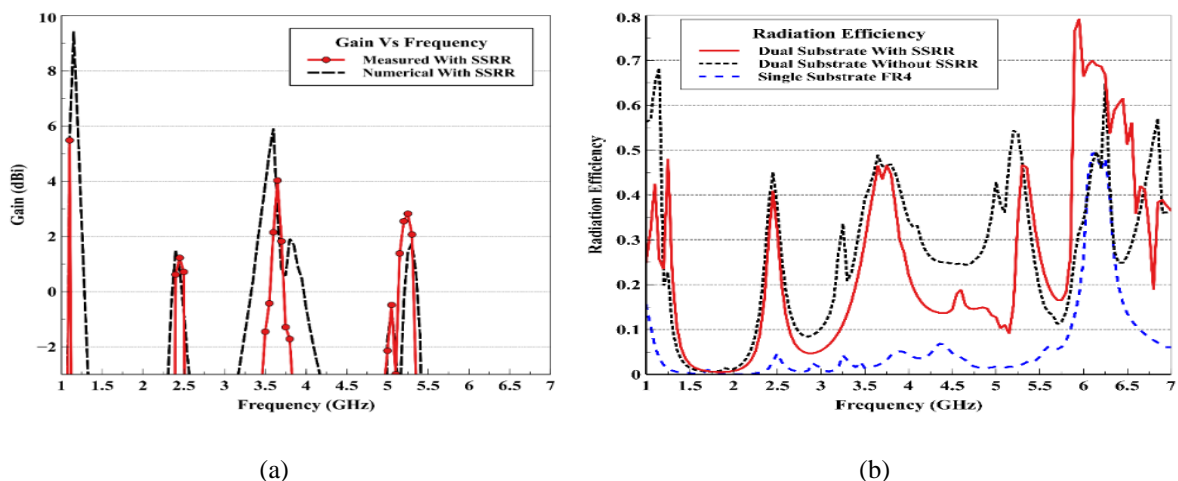


Figure 6. Characteristics of the patch antenna with embedded SSRR array, (a) Simulated and measured the gain of the antenna, (b) Plot of the radiation efficiency for single substrate (FR4), dual substrate without SSRR and dual substrate with SSRR structures

Table 4. Simulated and measured gain of the dual substrate patch antenna with embedded SSRR at various resonant frequencies

Frequency (GHz)	Gain (dBi)		Frequency (GHz)	Gain (dBi)	
	Simulated	Measured		Simulated	Measured
1.1	5.52	5.48	3.65	2.818	4.025
2.45	0.796	1.223	5.25	1.458	2.822

3.3. Current distribution on the antenna

Figure 7 shows the surface current distribution obtained from the HFSS simulation. The current distribution shows how the structure surface is excited by the current. The major contributors are the slots etched to provide longer current paths and the feedline of the patch. The current concentrates along the length of the slots (S11, S12 & S13). We observe that the current intensity is higher along the edges of slot S11 at almost all the frequencies. We position the slots S12 & S13 selectively by design to influence the current distribution at 1.1 & 3.65 GHz. The current concentration towards the feed line and slot edge is attributed to the patch's embedded resonator array. The resonators are excited at 2.45 GHz and 3.65 GHz and influence the current pattern on the patch largely.

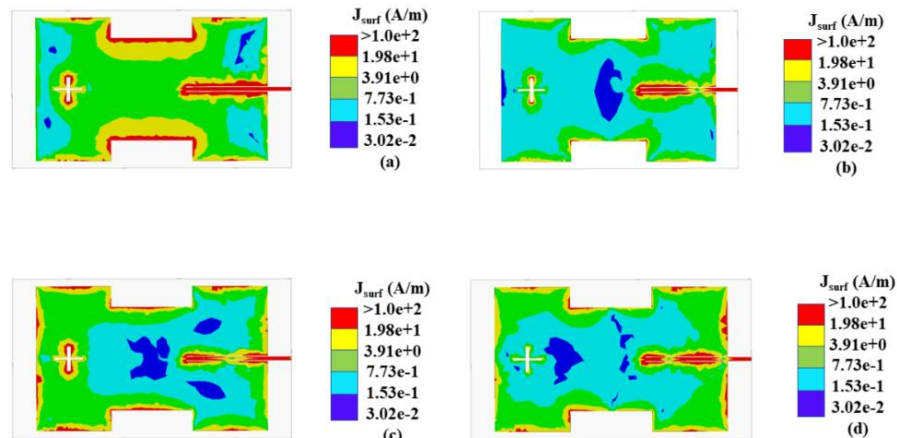


Figure 7. Surface distribution of current on the radiating surface of the patch antenna, (a) 1.1 GHz, (b) 2.45 GHz, (c) 3.65 GHz, (d) 5.25 GHz

3.4. Radiation pattern

Figure 8 in appendix, depicts the radiation pattern in the antenna's E and H planes at 1.1 GHz, 2.45 GHz, 3.65 GHz, and 5.25 GHz. The radiation pattern of the antenna exhibits a good correlation between the simulated and measured values. The pattern is dipolar in H-plane at 2.45 GHz, whereas it is omnidirectional in all other resonant frequencies (both E & H). The kinks/distortions observed in the measured value can be because of the coaxial connector's soldering with the patch, surface currents induced in the metallic inclusions in the multilayer structure influencing the radiation. The pattern measurement constrained by a protruded mounting mechanism hindering the values in particular radial.

3.5. Discussion

A list of a comparative study of a few of the research articles available concerning specific key parameters like frequency bands, substrate height, gain and number of substrates is in Table 5. The comparison brings out the uniqueness of the proposed structure visa-a-vie the ones published to date. The designed antenna operates in multiple frequency bands without alteration in the radiating patch's physical dimension. Secondly, it exhibits proper levels of gain on a thin substrate across all the resonant frequencies. Thirdly, an embedded SSRR array suppresses undesired frequencies and enhance radiation performance in other frequency bands. The most crucial factor is the technique of alignment and bonding of the two dielectric substrates. There is a chance of a shift in resonant frequency if the substrates are not appropriately aligned.

Table 5. Comparison table of antenna performance and design parameters of a few articles available in the literature and proposed work (*measured value)

Reference	Frequency Bands (GHz)	Thickness (mm)	No of Layers	Max Gain (dBi)	Feed Type	Configuration
[1]	0.8-6.05	0.8	1	5.35*	Meander Line	Single Substrate
[3]	2.4/3.5/5.2/5.8/8.2	1.6	1	3.49	CPW	Single Substrate
[4]	0.5-2.69/3.2-4.44/4.82-6.6	1.6	1	3.4	Inset	Single Substrate
[7]	8.64	1.5+1.3+1.3	3	3.24	Coaxial	Superstrate
[11]	2.45	2.34	2	~-1	Inset	Bonded
[12]	0.5/2/4/5.4	1.5748	2	NA	Inset	Bonded
[14]	1.9	2.307	2	-1.22*	CPW	Bonded
[16]	1/2	5.8	2	7.41	Inset	Bonded
[18]	9.25-11	1.6	1	7.85*	Microstrip line	Single Substrate
[20]	350-385	1	2	8.15*	Microstrip line	Dual CMOS Tech
[21]	20-120	0.13	1	15.11	Microstrip line	Single Substrate
[22]	0.5-6.4	1.6	1	5.3*	Microstrip line	Single Substrate
[25]	9.12-9.16	1.6	1	NA	Microstrip line	Single Substrate
[26]	8.7-11.7/11.9-14.6/15.6-17.1/22-26/29-34.2	1.6	1	9.15*	Microstrip line	Single Substrate
[27]	5.8	1.48+1.48	2	8.0*	Corporate	Superstrate
[35]	5.5/6.81/9.31	3.2	2	6.76*	Inset	Bonded
Proposed	1.1/2.45/3.65/5.25	0.908	2	5.48*	Inset	Bonded

4. CONCLUSION

The article does a detailed study of a microstrip patch antenna made of non-homogeneous substrate materials with an embedded SSRR array operating in 1.1, 2.45, 3.65 and 5.25 GHz bands. The numerical analysis and measurement of the prototype have shown very close agreement in the various performance parameters. The antenna's evolution from a single substrate to a dual substrate with embedded SSRR indicates improved performance indices of the vital parameters related to the antenna. The dual substrate feature aids in reducing the side length of the SSRR and makes it capable of resonating at lower frequencies, thereby bringing about a kind of frequency reconfigurability and compactness. The antenna produces maximum gain measured is 5.48 dBi at 1.1 GHz and the maximum bandwidth obtained is 60 MHz (1.2%) at 5.25 MHz on a thin substrate (0.908 mm). The proposed antenna produces output only in the required bands and suppresses unwanted resonances. The dual substrate antenna's performance in L-, S- and C- bands is encouraging and can be used in various wireless applications. Broadside radiation is noted in 1.1/3.65/5.25 GHz, while dipolar radiation pattern in H-plane at 2.45 GHz. The proposed design reduces 48% in patch length and 55% in patch width of the antenna.

APPENDIX

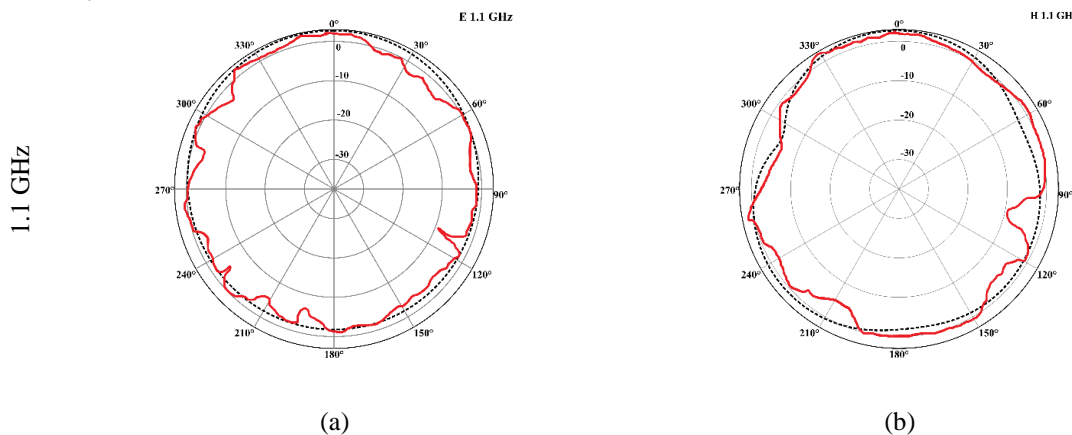


Figure 8. Radiation pattern of the microstrip patch antenna with embedded SSRR, (a) E-plane radiations at 1.1 GHz, 2.45 GHz, 3.67 & 5.26 GHz, (b) H-plane radiations at 1.1 GHz, 2.45 GHz, 3.67 & 5.26 GHz (legend-solid line-measured, dotted fine-simulated)

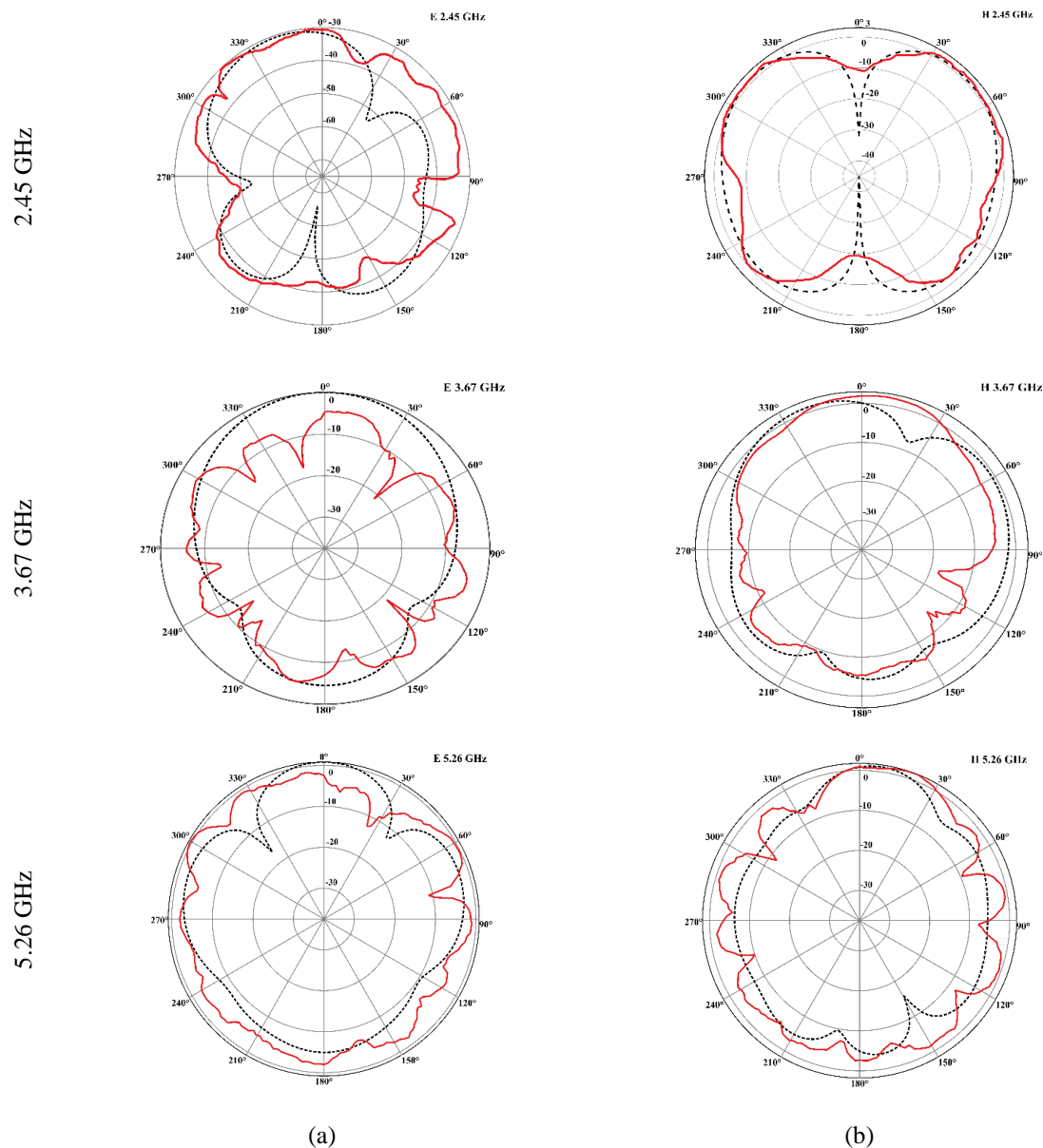


Figure 8. Radiation pattern of the microstrip patch antenna with embedded SSRR, (a) E-plane radiations at 1.1 GHz, 2.45 GHz, 3.67 & 5.26 GHz, (b) H-plane radiations at 1.1 GHz, 2.45 GHz, 3.67 & 5.26 GHz (legend-solid line-measured, dotted fine-simulated) (continue)

REFERENCES

- [1] M. Alibakhshi-Kenari, M. Naser-Moghadasi, R. A. Sadeghzadeh, B. S. Virdee, and E. Limiti, "Bandwidth Extension of planar antennas using embedded slits for reliable multiband RF communications," *AEU-International Journal of Electronics and Communications*, vol. 70, no. 7, pp. 910-919, 2016, doi: 10.1016/j.aeue.2016.04.003.
- [2] J. B. Pendry, A. J. Holden, D. J. Robbins and W. J. Stewart, "Magnetism from conductors and enhanced nonlinear phenomena," in *IEEE Transactions on Microwave Theory and Techniques*, vol. 47, no. 11, pp. 2075-2084, Nov. 1999, doi: 10.1109/22.798002.
- [3] R. Rajkumar and K. Usha Kiran, "A compact metamaterial multiband antenna for WLAN/WiMAX/ITU band applications," *AEU - International Journal of Electronics and Communications*, vol. 70, no. 5, pp. 599-604, 2016, doi: 10.1016/j.aeue.2016.01.025.
- [4] V. Rajeshkumar and S. Raghavan, "A compact metamaterial inspired triple-band antenna for reconfigurable WLAN/WiMAX applications," *AEU-International Journal of Electronics and Communications*, vol. 69, no. 1, pp. 274-280, 2014, doi: 10.1016/j.aeue.2014.09.012.
- [5] M. Alibakhshikenari, B. S. Virdee, and E. Limiti, "Triple-band planar dipole antenna for omnidirectional radiation," *Microwave and Optical Technology Letters*, vol. 60, no. 4, pp. 1048-1051, 2018, doi: 10.1002/mop.31098.

[6] H. Xiong, J. S. Hong, and Y. H. Peng, "Impedance bandwidth and gain improvement for microstrip antenna using metamaterials," *Radioengineering*, vol. 21, no. 4, pp. 993-998, 2012.

[7] S. K. Patel, C. Argyropoulos, and Y. P. Kosta, "Broadband compact microstrip patch antenna design loaded by multiple split ring resonator superstrate and substrate," *Waves in Random and Complex Media*, vol. 5030, no. 1, pp. 1-12, 2016, doi: 10.1080/17455030.2016.1203081.

[8] S. K. Patel and Y. Kosta, "Complementary split ring resonator metamaterial to achieve multifrequency operation in microstrip-based radiating structure design," *Journal of Modern Optics*, vol. 61, no. 3, pp. 249-256, 2014, doi: 10.1080/09500340.2013.879938.

[9] S. Nelaturi and N. Sarma, "Dual-Band Circular Patch Antenna based on Metamaterials," *IJAMT*, vol. 3, no. 2, pp. 152-155, 2018.

[10] R. O. Ouedraogo, E. J. Rothwell, A. R. Diaz, K. Fuchi and A. Temme, "Miniaturization of Patch Antennas Using a Metamaterial-Inspired Technique," in *IEEE Transactions on Antennas and Propagation*, vol. 60, no. 5, pp. 2175-2182, May 2012, doi: 10.1109/TAP.2012.2189699.

[11] R. O. Ouedraogo and E. J. Rothwell, "Metamaterial inspired patch antenna miniaturization technique," *2010 IEEE Antennas and Propagation Society International Symposium*, Toronto, ON, Canada, 2010, pp. 1-4, doi: 10.1109/APS.2010.5561205.

[12] J. C. Xing Zhao, Youngki Lee, "Design of Compact Patch Antenna Using Split-ring Resonator Embedded Substrate," *Microwave and Optical Technology Letters*, vol. 53, no. 12, pp. 2786-2790, 2011, doi: 10.1002/mop.26411.

[13] M. M. S. Kumar and P. I. Basarkod, "Design of a Dual-Substrate H-Type Patch Antenna for UHF RFID Applications," *2018 3rd IEEE International Conference on Recent Trends in Electronics, Information & Communication Technology (RTEICT)*, Bangalore, India, 2018, pp. 789-793, doi: 10.1109/RTEICT42901.2018.9012473.

[14] D. Mitra, B. Ghosh, A. Sarkhel and S. R. Bhadra Chaudhuri, "A Miniaturized Ring Slot Antenna Design With Enhanced Radiation Characteristics," in *IEEE Transactions on Antennas and Propagation*, vol. 64, no. 1, pp. 300-305, Jan. 2016, doi: 10.1109/TAP.2015.2496628.

[15] H. Malekpoor and M. Hamidkhani, "Compact multiband stacked circular patch antenna for wideband applications with enhanced gain," *Electromagnetics*, vol. 39, no. 4, pp. 241-253, 2019, doi: 10.1080/02726343.2019.1595379.

[16] C. D. R. R. Prasad Rao, Budumuru Srinu, "Design and Analysis of Multi Substrate Microstrip Patch Antenna," in *Microelectronics, Electromagnetics and Telecommunications: Proceedings of ICMEET 2015*, 2015, vol. 372, pp. 733-739, doi: 10.1007/978-81-322-2728-1_70.

[17] A. R. O. Mumin, R. Alias, J. Abdullah, S. H. Dahlan, J. Ali, and S. K. Debnath, "Design a compact square ring patch antenna with AMC for SAR reduction in WBAN applications," *Bulletin of Electrical Engineering and Informatics (BEEI)*, vol. 9, no. 1, pp. 370-378, 2020, doi: 10.11591/eei.v9i1.1686.

[18] M. Alibakhshikenari *et al.*, "Isolation enhancement of densely packed array antennas with periodic MTM-photonic bandgap for SAR and MIMO systems," *IET Microwaves, Antennas & Propagation*, vol. 14, no. 3, pp. 183-188, 2020, doi: 10.1049/iet-map.2019.0362.

[19] S. M. Shah *et al.*, "A 2.45 GHz microstrip antenna with harmonics suppression capability by using defected ground structure," *Bulletin of Electrical Engineering and Informatic (BEEI)s*, vol. 9, no. 1, pp. 387-395, 2020, doi: 10.11591/eei.v9i1.1847.

[20] M. Alibakhshikenari, B. S. Virdee, C. H. See, R. A. Abd-Alhameed, F. Falcone, and E. Limiti, "High-Gain Metasurface in Polyimide On-Chip Antenna Based on CRLH-TL for Sub-Terahertz Integrated Circuits," *Scientific Reports*, vol. 10, no. 1, pp. 1-9, 2020, doi: 10.1038/s41598-020-61099-8.

[21] M. Alibakhshikenari, B. S. Virdee, C. H. See, R. A. Abd-Alhameed, F. Falcone, and E. Limiti, "Super-wide impedance bandwidth planar antenna for microwave and millimetre-wave applications," *Sensors (Switzerland)*, vol. 19, no. 10, pp. 1-9, 2019, doi: 10.3390/s19102306.

[22] M. Alibakhshikenari *et al.*, "Double-Port Slotted-Antenna With Multiple Miniaturised Radiators for Wideband Wireless Communication Systems and Portable Devices," *Progress In Electromagnetics Research C*, vol. 90, pp. 1-13, 2019, doi: 10.2528/PIERC18011204.

[23] M. Alibakhshikenari, B. S. Virdee, C. H. See, R. A. Abd-Alhameed, F. Falcone and E. Limiti, "Surface wave reduction in antenna arrays using metasurface inclusion for MIMO and SAR systems," in *Radio Science*, vol. 54, no. 11, pp. 1067-1075, Nov. 2019, doi: 10.1029/2019RS006871.

[24] M. Alibakhshikenari, B. S. Virdee, and E. Limiti, "Study on isolation and radiation behaviours of a 34×34 array-antennas based on SIW and metasurface properties for applications in terahertz band over 125–300 GHz," *Optik*, vol. 206, p. 163222, 2020, doi: 10.1016/j.ijleo.2019.163222.

[25] M. Alibakhshikenari, M. Khalily, B. S. Virdee, C. H. See, R. A. Abd-Alhameed and E. Limiti, "Mutual-Coupling Isolation Using Embedded Metamaterial EM Bandgap Decoupling Slab for Densely Packed Array Antennas," in *IEEE Access*, vol. 7, pp. 51827-51840, 2019, doi: 10.1109/ACCESS.2019.2909950.

[26] M. Alibakhshikenari, M. Khalily, B. S. Virdee, C. H. See, R. A. Abd-Alhameed and E. Limiti, "Mutual Coupling Suppression Between Two Closely Placed Microstrip Patches Using EM-Bandgap Metamaterial Fractal Loading," in *IEEE Access*, vol. 7, pp. 23606-23614, 2019, doi: 10.1109/ACCESS.2019.2899326.

[27] C. Arora, S. S. Pattnaik, and R. N. Baral, "SRR Superstrate for Gain and Bandwidth Enhancement of Microstrip Patch Antenna Array," *Progress In Electromagnetics Research B*, vol. 76, no. May, pp. 73-85, 2017, doi: 10.2528/PIERB17041405.

[28] T. Ali, S. Pathan, and R. C. Biradar, "A Miniaturized Circularly Polarised Coaxial Fed Superstrate Slot Antenna for

L-band Application," *Internet Technology Letters*, vol. 1, no. 6, 2018, doi: 10.1002/itl2.21.

[29] B. Constantine A., "Antenna Theory Analysis and Design Third Edition," Third. Wiley-Interscience, 2005.

[30] Z. Szabó, G. Park, R. Hedge and E. Li, "A Unique Extraction of Metamaterial Parameters Based on Kramers-Kronig Relationship," in *IEEE Transactions on Microwave Theory and Techniques*, vol. 58, no. 10, pp. 2646-2653, Oct. 2010, doi: 10.1109/TMTT.2010.2065310.

[31] D. R. Smith, S. Schultz, P. Markoš, and C. M. Soukoulis, "Determination of effective permittivity and permeability of metamaterials from reflection and transmission coefficients," *Physical review B* vol. 65, pp. 1-5, 2002.

[32] D. R. Smith, D. C. Vier, T. Koschny, and C. M. Soukoulis, "Electromagnetic parameter retrieval from inhomogeneous metamaterials," *Physical Review E*, vol. 71, no. 3, pp. 1-11, 2005.

[33] H. Chen, L. Ran, J. Huangfu, X. Zhang, and K. Chen, "Left-handed materials composed of only S-shaped resonators," *Physical review E*, vol. 057605, no. 70, pp. 1-4, 2004.

[34] A. M. Shalini Sah and Malay R Tripathi, "Multiband and Miniaturised dual-layer Antenna incorporated with FSS and DGS," *Advanced Electromagnetics*, vol. 7, no. 1, pp. 1-6, 2018, doi: 10.7716/aem.v7i1.534.

[35] D. Chaturvedi and S. Raghavan, "SRR-loaded metamaterial-inspired electrically-small monopole antenna," *Progress In Electromagnetics Research*, vol. 81, pp. 11-19, 2018, doi: 10.2528/PIERC17101202.

[36] F. Bilotti, A. Toscano, L. Vegni, K. Aydin, K. B. Alici and E. Ozbay, "Equivalent-Circuit Models for the Design of Metamaterials Based on Artificial Magnetic Inclusions," in *IEEE Transactions on Microwave Theory and Techniques*, vol. 55, no. 12, pp. 2865-2873, Dec. 2007, doi: 10.1109/TMTT.2007.909611.

[37] N. Saranya and T. Kesavamurthy, "Design and performance analysis of broadband rectenna for an efficient RF energy harvesting application," *International Journal of RF and Microwave Computer-Aided Engineering*, vol. 29, no. 1, pp. 1-12, 2019, doi: 10.1002/mmce.21628.

[38] A. B. Numan and M. S. Sharawi, "Extraction of Material Parameters for Metamaterials Using a Full-Wave Simulator [Education Column]," in *IEEE Antennas and Propagation Magazine*, vol. 55, no. 5, pp. 202-211, Oct. 2013, doi: 10.1109/MAP.2013.6735515.

[39] M. S. Kumar and P. I. Basarkod, "A Study of the Effect of Dielectric Composition on Metamaterial Performance in a Multilayer Environment," *2019 International Conference on Data Science and Communication (IconDSC)*, Bangalore, India, 2019, pp. 1-5, doi: 10.1109/IconDSC.2019.8817012.

BIOGRAPHIES OF AUTHORS



M Shailesh Rao is a graduate & postgraduate in Electrical Engineering. An experienced professional in radar and telecommunication engineering domains with more than 25+ years of exposure. At present, he is a research scholar and working towards his PhD at REVA University, Bengaluru. His areas of interest are antennas, computational Electromagnetics, radar engineering and photonics.



Dr Prabhugoud I. Basarkod, Professor, School of Electronics and Communication Engineering. He has 30+ years of teaching and research experience. He has many research publications in reputed national/international journals and conferences. His research areas of interests include Wireless Networks, Mobile Ad hoc Networks (MANETs), Agent technology, Multimedia communication, antennas, and wireless sensor networks. He is a member of the Indian Society for Technical Education, Institute of Electrical and Electronics Engineers (IEEE), Member Institution of Electronics, and Institution of Electronics and Telecommunication Engineers (IETE).